Journal of Systems Engineering and Electronics
Vol. 31, No. 5, October 2020, pp.1041 – 1050

Sliding-mode control for a rolling-missile with input constraints

HUA Siyu[1,*], WANG Xugang[2,*], and ZHU Yin[2]

1. The 802 Institute of Shanghai Academy of Space Flight Technology, Shanghai 201100, China;
2. School of Energy and Power Engineering, Nanjing University of Science and Technology, Nanjing 210094, China

Abstract: This paper investigates the overload stabilization problem of the rolling-missile subject to parameters uncertainty and actuator saturation. In order to solve this problem, a sliding-mode control (SMC) scheme is technically employed by using the back-stepping approach to make the dynamic system stable. In addition, SMC with the tanh-type switching function plays an important role in reducing intrinsic vibration. Furthermore, an auxiliary system (AS) is developed to compensate for nonlinear terms arising from input saturation. Finally, the simulation results provide a solution to demonstrate that the suggested SMC and the AS methodology have advantages of strong tracking capability, anti-interference ability and anti-saturation performance.

Keywords: input constraint, back-stepping approach, sliding-mode control (SMC), auxiliary control system.

DOI: 10.23919/JSEE.2020.000078

1. Introduction

In many current and future missions, not only guidance accuracy is needed, but also a control system is required to trace guidance command correctly and rapidly to guarantee expected motion for a rolling-missile. Its oblique tail can provide a rolling-speed that leads to a strong coupling between pitch-channel and yaw-channel motions. Additionally, its aerodynamic coefficients have some uncertainty, and the actuator may be easier to fall into a saturated state, which is an enormous challenge for precision attack missions.

On the one hand, in order to address nonlinear issues on parameters uncertainty, many scholars have done deeply research, and a lot of effective control methods [1 – 11], such as back-stepping technique, sliding-mode control (SMC), adaptive control and robust control, have been proposed.

Dong et al. [1] presented a switched controller based on a fuzzy logic system for near space vehicles containing unknown disturbances and uncertainties, where total disturbances were compensated by adopting the back-stepping method, and given examples showed the effectiveness and advantages of the proposed control method. Dian et al. [2] utilized an approximator to approximate unknown and nonlinear functions, which guaranteed tracking errors to be ultimately bounded. Jiang et al. [3] proposed an adaptive back-stepping method and SMC for flight attitude of quadrotor UAVs, which stabilized their attitude and had hover flight capabilities under perturbations and external disturbances. For a quadrotor micro aerial vehicle under external perturbations, an adaptive second order SMC was designed by Herman et al. [4], and simulation results showed its feasibility and attractiveness. In [5], for an aircraft with external disturbances, the proposed SMC removed a chattering effect, revealed significant adaptive properties and guaranteed precise constraint fulfillment within a finite time. In [6], for the problem of attitude control of a quad tilt rotor aircraft with unknown external disturbances, a new exponential fast nonsingular terminal sliding surface was proposed, which achieved a good control performance. In [7], a hyperbolic tangent function played a role in vibration reduction in the SMC system. Zhang et al. [8] proposed a global SMC for UAVs against parameter uncertainties and external disturbances, eventually eliminating intrinsic vibration in the SMC scheme. Zheng et al. [9] presented an adaptive back-stepping controller to improve performances by more than 80% compared with passive vehicle suspension systems. In [10], using both adaptive sliding surfaces and adaptive controller was able to manage input disturbances with bounded derivatives. In [11], a robust decentralized fault-tolerant resilient controller was designed to compensate for both actuator fault and input saturation, and simulation results showed great robustness of the designed control scheme.

On the other hand, actuator saturation as a dominant input nonlinearity often limits system performance and severely leads to its instability [12]. As showed in [13], ac-

Manuscript received June 05, 2019.
*Corresponding author.
This work was supported by the Fundamental Research Funds for the Central Universities (30919011401).

tuator saturation means that output of an actuator is limited to physical constraints, which makes actual output smaller than control input given by the designed controller. As a result, the designed controller loses the ability to adjust control output in time, which makes the control system unstable. In [14], actuator saturation included input magnitude and rate saturation. Input magnitude saturation is the key research in this paper.

As shown in [15 – 29], there are three major approaches to handling input constraints, including Nussbaum-type technique, anti-windup control (AWC) and auxiliary system (AS).

In terms of Nussbaum-type technique, loads of scholars made some experiments. Liang [15] designed a robust adaptive control law of guidance and control system for a missile with input constraints. To address this problem, the Nussbaum function was employed, eventually making saturation function smooth. Hu et al. [16] proposed an attitude control scheme incorporating the Nussbaum gain technique into back-stepping design for a spacecraft, compensating for time-varying nonlinear terms arising from input saturation. In [17], a Nussbaum-type function-based dead-zone model was introduced, and results demonstrated its tracking performance.

What's more, AWC is also effective. Hussain et al. [18] presented a robust nonlinear dynamic AWC design for nonlinear systems with parametric uncertainties and actuator saturation, and simulation results showed that the suggested AWC methodology was able to compensate for saturation and effectively deal with parametric uncertainties. Liu et al. [19] proposed a novel AWC based on robust tracking control, and simulation study was carried out to illustrate its anti-saturation ability and great tracking performance. In [20], a robust anti-windup controller was adopted for an in-plane motion, which showed some advantages. In [21], input saturation was solved by designing an AWC, and simulation results demonstrated its effectiveness. For a class of aircraft, a Riccati-based AWC was employed to solve the input saturation problem in [22]. Static AWC was designed for uncertain linear systems to deal with input saturation [23]. He et al. [24] proposed one-step AWC, and simulation results verified its effectiveness and feasibility.

In addition, AS is available. For an unmanned surface vehicle, Wang et al. [25] proposed an anti-saturation auxiliary function to compensate for the magnitude and rate saturation of the rudder. In [26], an AS was constructed to analyze and compensate for the effect of input saturation. Tao et al. [27] developed a novel AS for a flexible spacecraft to compensate for adverse effects of actuator saturation. In [28] and [29], the AS technique was proposed for an uncertain multiple-input-multiple-output (MIMO) nonlinear system with input constraints, and simulation studies were presented to illustrate its effectiveness and priority.

In this paper, we follow SMC and AS approaches, designing a controller which achieves high-precision stabilization of a rolling-missile. To address the issues on parameters uncertainty, back-stepping technique and SMC are both necessary. To compensate for nonlinear terms arising from input constraints, a special AS is used.

The remainder of this paper is organized as follows. In Section 2, we adopt a kinetic model called "standard block-controlled type" system in [30], which is prepared for using the back-stepping approach to design the SMC law. Section 3 introduces a new control scheme containing a virtual control law and an actual control law, which improves its convergence behavior and its ability against parameters perturbation, and this part also illustrates the AS technique towards input saturation. Section 4 shows illustrative numerical examples of the proposed controller. Concluding remarks are provided in Section 5.

2. System description

In this paper the low-speed rolling-missile with canards is our study subject. Maneuvering "cross rudder" can change its pitch-channel and yaw-channel motions. Additionally, its oblique tail can provide a stable rolling-speed for a rolling-missile to assure its dual-channel stability. The following assumptions are adopted:

(i) Aerodynamic forces are axisymmetric.

(ii) Errors influenced by their structure can be ignored. Its mass is symmetric about the longitudinal axis.

(iii) It conforms to "small disturbances".

The defined state variables of the dynamic system are $\boldsymbol{X}_1 = [n_y \quad n_z]^{\mathrm{T}}$, $\boldsymbol{X}_2 = [\omega_y \quad \omega_z]^{\mathrm{T}}$, and the defined input variable of the dynamic system is $\boldsymbol{U} = [\delta_y \quad \delta_z]^{\mathrm{T}}$. Furthermore, this dynamic system for a rolling-missile can be described as the following "standard block-controlled type" system:

$$\begin{cases} \dot{\boldsymbol{X}}_1 = \boldsymbol{F}_1(\boldsymbol{X}_1) + \boldsymbol{G}_1(\boldsymbol{X}_1)\boldsymbol{X}_2 + \boldsymbol{D}_1 \\ \dot{\boldsymbol{X}}_2 = \boldsymbol{F}_2(\boldsymbol{X}_1, \boldsymbol{X}_2) + \boldsymbol{G}_2(\boldsymbol{X}_2)\boldsymbol{U} + \boldsymbol{D}_2 \end{cases} \tag{1}$$

where

$$\boldsymbol{F}_1(\boldsymbol{X}_1) = \begin{bmatrix} -\overline{a}_{34} n_y \\ -\overline{a}_{34} n_z \end{bmatrix},$$

$$\boldsymbol{F}_2(\boldsymbol{X}_1, \boldsymbol{X}_2) = \begin{bmatrix} \overline{a}_{22}\omega_y - \dfrac{g a_{24}}{v a_{34}} n_z + \dfrac{g a'_{27}}{v a_{34}} n_y - a'_{28}\omega_z \\ \overline{a}_{22}\omega_z + \dfrac{g a_{24}}{v a_{34}} n_y + \dfrac{g a'_{27}}{v a_{34}} n_z + a'_{28}\omega_z \end{bmatrix},$$

$$\boldsymbol{G}_1(\boldsymbol{X}_1) = \begin{bmatrix} 0 & \dfrac{v}{g} a_{34} \\ -\dfrac{v}{g} a_{34} & 0 \end{bmatrix},$$

$$\boldsymbol{G}_2(\boldsymbol{X}_2)=\begin{bmatrix}\overline{a}_{25} & 0\\ 0 & \overline{a}_{25}\end{bmatrix},$$

$$\boldsymbol{D}_1=\begin{bmatrix}\Delta a_{34}n_y+\dfrac{v}{g}a_{34}a_{35}\delta_z\\ \Delta a_{34}n_z-\dfrac{v}{g}a_{34}a_{35}\delta_y\end{bmatrix},$$

$$\boldsymbol{D}_2=\begin{bmatrix}\Delta a_{22}\omega_y+\Delta a_{25}\delta_y\\ \Delta a_{22}\omega_z+\Delta a_{25}\delta_z\end{bmatrix}.$$

Symbols appearing above are given in Table 1.

Table 1 Symbolic definitions of the dynamic system

Symbol	Definition
v	Flight velocity
δ_y, δ_z	Elevator angle, rudder angle
n_y, n_z	Longitudinal overload, lateral overload
ω_y, ω_z	Pitch angular rate, yaw rate
a_{22}, a_{24}, a_{25}, a_{34}, a_{35}	Aerodynamic coefficients
"$-$", "Δ"	Nominal value of the parameter, perturbation value of the parameter
$\boldsymbol{D}_1$, $\boldsymbol{D}_2$	Uncertainty

3. SMC and AS design approach

In this section, our goal is to provide how to design SMC and AS for this "standard block-controlled type" system of (1). Design steps are divided into three steps as follows:

(i) According to (1), we design the zero-order SMC surface to obtain error equations. The adopting back-stepping method is to design a virtual control law of SMC. Desired state variables of the dynamic system are designed for a virtual control law of SMC, which makes the tracking errors of overload converge to the origin or its small neighborhood, meanwhile, stability of the SMC system is proved based on the Lyapunov theory.

(ii) To make the tracking errors of angular rates converge to the origin or its small neighborhood, we can get another error equations and design an actual control law of SMC in a similar way as in step (i), meanwhile, the proof of stability of the SMC system is given. Step (i) and Step (ii) constitute a complete SMC design.

(iii) Based on (1), AS can be designed. In order to address the issue on input constraints, systematic errors caused by actuator saturation are designed for state variables of AS. Moreover, state variables of the dynamic system are fed into SMC. Finally, stability proof of AS is given.

The architecture for this control system is shown in Fig. 1. In Fig. 1, $\boldsymbol{y}_c$ is the input variable of this novel SMC system, including expected overload and angular rates, which is obtainable from guidance loop. $\boldsymbol{y}$ is the output variable of this SMC system. $\boldsymbol{U}$ is the SMC law. $\mathrm{sat}(\boldsymbol{U})$ is the plant's changed input caused by the actuator's saturation. $\boldsymbol{E}$ and $\Delta\boldsymbol{u}$ are output and input variables of AS respectively.

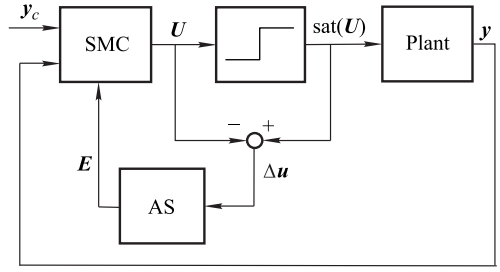

Fig. 1 Illustration of a novel SMC system

3.1 Design of a virtual control law of SMC

To simplify the design of this control law, assumptions and lemmas are given as follows.

Assumption 1 $\|\boldsymbol{G}_1(\boldsymbol{X}_1)\boldsymbol{S}_2\|+\|\boldsymbol{D}_1\|\leqslant\rho_1$ is true in this dynamic model. ρ_1 is an unknown, bounded and positive number.

Lemma 1 In [31], there are positive numbers $\alpha_m,\beta_m,\theta_m\in\mathbf{R}$, so that $\boldsymbol{G}_1(\boldsymbol{X}_1)$ can be invertible for all α, β, $\theta\in\mathbf{R}$ that satisfy $|\alpha|\leqslant\alpha_m$, $|\beta|\leqslant\beta_m$ and $|\theta|\leqslant\theta_m$.

Lemma 2 Let $\boldsymbol{A}$ and $\boldsymbol{B}$ be diagonal matrixes. $\lambda_{\min}(\boldsymbol{AB})$, $\lambda_{\min}(\boldsymbol{A})$ and $\lambda_{\min}(\boldsymbol{B})$ are minimum eigenvalues of $\boldsymbol{AB}$, $\boldsymbol{A}$ and $\boldsymbol{B}$ respectively, then $\lambda_{\min}(\boldsymbol{AB})=\lambda_{\min}(\boldsymbol{A})\lambda_{\min}(\boldsymbol{B})$ is true.

Lemma 3 If $\lambda_{\min}(\boldsymbol{k}_1)$ is the minimum eigenvalue of matrix $\boldsymbol{k}_1$, then $\boldsymbol{S}_1^{\mathrm{T}}(\boldsymbol{k}_1\boldsymbol{S}_1)\geqslant\lambda_{\min}(\boldsymbol{k}_1)\|\boldsymbol{S}_1\|^2$ is true.

In this section, designing the zero-order SMC surface can promote poor anti-interference ability of the traditional SMC law. Let expected longitudinal and lateral overload signals be n_{yd},n_{zd} and the expected yaw and pitch angular rate signals be ω_{yd},ω_{zd}. Hence, zero-order SMC surfaces $\boldsymbol{S}_1,\boldsymbol{S}_2\in\mathbf{R}^2$ and their expressions are

$$\begin{cases}\boldsymbol{S}_1=\boldsymbol{X}_1-\boldsymbol{X}_{1d}\\ \boldsymbol{S}_2=\boldsymbol{X}_2-\boldsymbol{X}_{2d}\end{cases}\tag{2}$$

where

$$\boldsymbol{X}_{1d}=[n_{yd}\quad n_{zd}]^{\mathrm{T}},\boldsymbol{X}_{2d}=[\omega_{yd}\quad\omega_{zd}]^{\mathrm{T}},$$

$$\boldsymbol{S}_1=[S_{11}\quad S_{12}]^{\mathrm{T}},\boldsymbol{S}_2=[S_{21}\quad S_{22}]^{\mathrm{T}}.$$

Error equations can be obtained from (1) and (2):

$$\dot{\boldsymbol{S}}_1=\boldsymbol{F}_1(\boldsymbol{X}_1)+\boldsymbol{G}_1(\boldsymbol{X}_1)\boldsymbol{S}_2+\boldsymbol{G}_1(\boldsymbol{X}_1)\boldsymbol{X}_{2d}+\boldsymbol{D}_1-\dot{\boldsymbol{X}}_{1d}.\tag{3}$$

Because of unknown $\boldsymbol{S}_2$, $\boldsymbol{G}_1(\boldsymbol{X}_1)\boldsymbol{S}_2$ is defined as an uncertainty, and $\boldsymbol{X}_{2d}$ is designed to be a virtual control law $\boldsymbol{\Omega}$:

$$\boldsymbol{\Omega}=\boldsymbol{G}_1(\boldsymbol{X}_1)^{-1}[-\boldsymbol{k}_1\boldsymbol{S}_1-\boldsymbol{F}_1(\boldsymbol{X}_1)-\boldsymbol{\Lambda}_1\boldsymbol{\Gamma}(\boldsymbol{S}_1)\boldsymbol{S}_1+\dot{\boldsymbol{X}}_{1d}]\tag{4}$$

where

$$\boldsymbol{k}_1 = \mathrm{diag}[k_{11}, k_{12}], \quad k_{11} > 0; k_{12} > 0,$$
$$\boldsymbol{\Lambda}_1 = \mathrm{diag}[\Lambda_{11}, \Lambda_{12}], \quad \Lambda_{11} > 0; \Lambda_{12} > 0,$$
$$\boldsymbol{\Gamma}(\boldsymbol{S}_1) = \mathrm{diag}[\tanh(\mu_1^{-1} S_{11}), \tanh(\mu_1^{-1} S_{12})], \quad \mu_1 > 1.$$

The first Lyapunov function is defined as

$$V_1 = \frac{1}{2} \boldsymbol{S}_1^{\mathrm{T}} \boldsymbol{S}_1. \tag{5}$$

Next, deriving V_1 we get

$$\dot{V}_1 = \boldsymbol{S}_1^{\mathrm{T}} \dot{\boldsymbol{S}}_1. \tag{6}$$

Substituting (3) into (6), we obtain

$$\dot{V}_1 = \boldsymbol{S}_1^{\mathrm{T}} [\boldsymbol{F}_1(\boldsymbol{X}_1) + \boldsymbol{G}_1(\boldsymbol{X}_1)\boldsymbol{S}_2 + \boldsymbol{G}_1(\boldsymbol{X}_1)\boldsymbol{X}_{2d} + \boldsymbol{D}_1 - \dot{\boldsymbol{X}}_{1d}]. \tag{7}$$

Substituting (4) into (7) and simplifying it, we get

$$\dot{V}_1 = \boldsymbol{S}_1^{\mathrm{T}} [\boldsymbol{G}_1(\boldsymbol{X}_1)\boldsymbol{S}_2 + \boldsymbol{D}_1 - \boldsymbol{k}_1 \boldsymbol{S}_1 - \boldsymbol{\Lambda}_1 \boldsymbol{\Gamma}(\boldsymbol{S}_1)\boldsymbol{S}_1]. \tag{8}$$

By referring to Assumption 1, we obtain

$$\boldsymbol{S}_1^{\mathrm{T}} [\boldsymbol{G}_1(\boldsymbol{X}_1)\boldsymbol{S}_2 + \boldsymbol{D}_1] \leqslant \|\boldsymbol{S}_1^{\mathrm{T}}\| [\|\boldsymbol{G}_1(\boldsymbol{X}_1)\boldsymbol{S}_2\| + \|\boldsymbol{D}_1\|] = \|\boldsymbol{S}_1\| [\|\boldsymbol{G}_1(\boldsymbol{X}_1)\boldsymbol{S}_2\| + \|\boldsymbol{D}_1\|] \leqslant \|\boldsymbol{S}_1\| \rho_1. \tag{9}$$

Let $\lambda_{\min}(\boldsymbol{k}_1)$ be the minimum eigenvalue of known diagonal matrix $\boldsymbol{k}_1$. According to Lemma 3, we acquire

$$-\boldsymbol{S}_1^{\mathrm{T}} \boldsymbol{k}_1 \boldsymbol{S}_1 \leqslant -\lambda_{\min}(\boldsymbol{k}_1) \|\boldsymbol{S}_1\|^2. \tag{10}$$

Similarly, let $\lambda_{\min}(\boldsymbol{\Lambda}_1)$ and $\lambda_{\min}(\boldsymbol{\Gamma}(\boldsymbol{S}_1))$ be the minimum eigenvalues of known diagonal matrices $\boldsymbol{\Lambda}_1$ and $\boldsymbol{\Gamma}(\boldsymbol{S}_1)$ respectively. According to Lemma 2 and Lemma 3, we acquire

$$-\boldsymbol{S}_1^{\mathrm{T}} \boldsymbol{\Lambda}_1 \boldsymbol{\Gamma}(\boldsymbol{S}_1)\boldsymbol{S}_1 = -\boldsymbol{S}_1^{\mathrm{T}} (\boldsymbol{\Lambda}_1 \boldsymbol{\Gamma}(\boldsymbol{S}_1)\boldsymbol{S}_1) \leqslant -\lambda_{\min}(\boldsymbol{\Lambda}_1 \boldsymbol{\Gamma}(\boldsymbol{S}_1)) \|\boldsymbol{S}_1\|^2 = -\lambda_{\min}(\boldsymbol{\Lambda}_1)\lambda_{\min}(\boldsymbol{\Gamma}(\boldsymbol{S}_1)) \|\boldsymbol{S}_1\|^2. \tag{11}$$

Substituting (9)–(11) into (8), we get

$$\dot{V}_1 = \boldsymbol{S}_1^{\mathrm{T}} [\boldsymbol{G}_1(\boldsymbol{X}_1)\boldsymbol{S}_2 + \boldsymbol{D}_1 - \boldsymbol{k}_1 \boldsymbol{S}_1 - \boldsymbol{\Lambda}_1 \boldsymbol{\Gamma}(\boldsymbol{S}_1)\boldsymbol{S}_1] \leqslant \|\boldsymbol{S}_1\| \rho_1 - \lambda_{\min}(\boldsymbol{k}_1) \|\boldsymbol{S}_1\|^2 - \lambda_{\min}(\boldsymbol{\Lambda}_1) \cdot \lambda_{\min}(\boldsymbol{\Gamma}(\boldsymbol{S}_1)) \|\boldsymbol{S}_1\|^2 = -[\lambda_{\min}(\boldsymbol{k}_1) + \lambda_{\min}(\boldsymbol{\Lambda}_1)\lambda_{\min}(\boldsymbol{\Gamma}(\boldsymbol{S}_1))] \|\boldsymbol{S}_1\|^2 + \|\boldsymbol{S}_1\| \rho_1. \tag{12}$$

Select the parameters of a virtual controller based on the inverted-U property of the mono basic quadratic function whose peak is a small and positive number, less than or equal to zero, which are described as

$$\begin{cases} -[\lambda_{\min}(\boldsymbol{k}_1) + \lambda_{\min}(\boldsymbol{\Lambda}_1)\lambda_{\min}(\boldsymbol{\Gamma}(\boldsymbol{S}_1))] < 0 \\ \dfrac{\rho_1^2}{4[\lambda_{\min}(\boldsymbol{k}_1) + \lambda_{\min}(\boldsymbol{\Lambda}_1)\lambda_{\min}(\boldsymbol{\Gamma}(\boldsymbol{S}_1))]} = \tau_1 \end{cases} \tag{13}$$

or

$$\begin{cases} -[\lambda_{\min}(\boldsymbol{k}_1) + \lambda_{\min}(\boldsymbol{\Lambda}_1)\lambda_{\min}(\boldsymbol{\Gamma}(\boldsymbol{S}_1))] < 0 \\ \dfrac{\rho_1^2}{4[\lambda_{\min}(\boldsymbol{k}_1) + \lambda_{\min}(\boldsymbol{\Lambda}_1)\lambda_{\min}(\boldsymbol{\Gamma}(\boldsymbol{S}_1))]} \leqslant 0 \end{cases}. \tag{14}$$

Because eigenvalues of this diagonal matrix $\boldsymbol{\Gamma}(\boldsymbol{S}_1) = \mathrm{diag}[\tanh(\mu_1^{-1} S_{11}), \tanh(\mu_1^{-1} S_{12})]$ are $\tanh(\mu_1^{-1} S_{11})$ and $\tanh(\mu_1^{-1} S_{12})$, we get $\lambda(\boldsymbol{\Gamma}(S_1)) = [-1, 1]$ easily. Hence, (13) is simplified to

$$\begin{cases} \lambda_{\min}(\boldsymbol{k}_1) > \lambda_{\min}(\boldsymbol{\Lambda}_1) > 0 \\ \dfrac{\rho_1^2}{4[\lambda_{\min}(\boldsymbol{k}_1) + \lambda_{\min}(\boldsymbol{\Lambda}_1)\lambda_{\min}(\boldsymbol{\Gamma}(\boldsymbol{S}_1))]} = \tau_1 \end{cases}. \tag{15}$$

Let $\phi = \dot{V}_1$ and $l = \|\boldsymbol{S}_1\|$, by taking (12) we acquire

$$\phi = -[\lambda_{\min}(\boldsymbol{k}_1) + \lambda_{\min}(\boldsymbol{\Lambda}_1)\lambda_{\min}(\boldsymbol{\Gamma}(\boldsymbol{S}_1))] l^2 + l\rho_1. \tag{16}$$

Relation between l and ϕ is shown in Fig. 2.

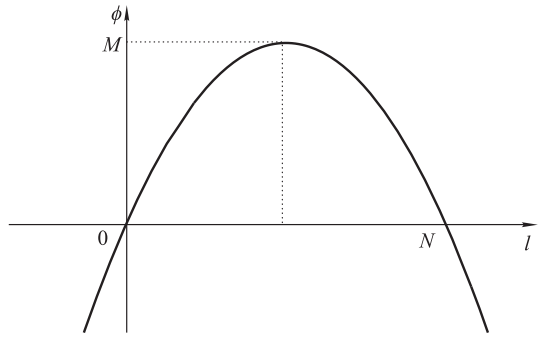

Fig. 2 A mono basic quadratic function

In Fig. 2, the ϕ-coordinate value of point M is

$$\frac{\rho_1^2}{4[\lambda_{\min}(\boldsymbol{k}_1) + \lambda_{\min}(\boldsymbol{\Lambda}_1)\lambda_{\min}(\boldsymbol{\Gamma}(\boldsymbol{S}_1))]},$$

and the l-coordinate value of point N is

$$\frac{\rho_1}{\lambda_{\min}(\boldsymbol{k}_1) + \lambda_{\min}(\boldsymbol{\Lambda}_1)\lambda_{\min}(\boldsymbol{\Gamma}(\boldsymbol{S}_1))}.$$

There are some characteristics analyzed as follows.

If $\|\boldsymbol{S}_1\| > \dfrac{\rho_1}{\lambda_{\min}(\boldsymbol{k}_1)+\lambda_{\min}(\boldsymbol{\Lambda}_1)\lambda_{\min}(\boldsymbol{\Gamma}(\boldsymbol{S}_1))}$, there is

$$\dot{V}_1 < 0. \tag{17}$$

If $\|\boldsymbol{S}_1\| \leqslant \dfrac{\rho_1}{\lambda_{\min}(\boldsymbol{k}_1)+\lambda_{\min}(\boldsymbol{\Lambda}_1)\lambda_{\min}(\boldsymbol{\Gamma}(\boldsymbol{S}_1))}$, there is

$$\dot{V}_1 \leqslant \tau_1. \tag{18}$$

It shows that if $\boldsymbol{S}_2$ is bounded, $\boldsymbol{S}_1$ is finally stable and bounded under the influence of a virtual control law, that is,

$$\|\boldsymbol{S}_1\| \leqslant \frac{\rho_1}{\lambda_{\min}(\boldsymbol{k}_1)+\lambda_{\min}(\boldsymbol{\Lambda}_1)\lambda_{\min}(\boldsymbol{\Gamma}(\boldsymbol{S}_1))}. \tag{19}$$

This virtual control law has no effects on convergence of $\boldsymbol{S}_2$. Therefore, it is substantial to design an actual control law to ensure convergence of $\boldsymbol{S}_2$.

3.2 Design of an actual control law of SMC

To simplify the design of an actual control law, assumptions and lemmas are given as follows.

Assumption 2 $\|\dot{\boldsymbol{X}}_{2d}\| \leqslant \rho_2$ is true in this dynamic model. ρ_2 is an unknown, bounded and positive number.

From (1) and (2), error equations can be obtained:

$$\dot{\boldsymbol{S}}_2 = \boldsymbol{F}_2(\boldsymbol{X}_1,\boldsymbol{X}_2)+\boldsymbol{G}_2(\boldsymbol{X}_2)\boldsymbol{U}+\boldsymbol{D}_2-\dot{\boldsymbol{X}}_{2d}. \tag{20}$$

Design this actual control law:

$$\boldsymbol{U} = \boldsymbol{G}_2(\boldsymbol{X}_2)^{-1}(-\boldsymbol{k}_2\boldsymbol{S}_2-\boldsymbol{F}_2(\boldsymbol{X}_1,\boldsymbol{X}_2)- \boldsymbol{\Lambda}_2\boldsymbol{\Gamma}(\boldsymbol{S}_2)\boldsymbol{S}_2+\dot{\boldsymbol{X}}_{2d}) \tag{21}$$

where

$$\boldsymbol{k}_2 = \mathrm{diag}[k_{21},k_{22}],\quad k_{21}>0; k_{22}>0,$$

$$\boldsymbol{\Lambda}_2 = \mathrm{diag}[\Lambda_{21},\Lambda_{22}],\quad \Lambda_{21}>0;\Lambda_{22}>0,$$

$$\boldsymbol{\Gamma}(S_2) = \mathrm{diag}[\tanh(\mu_2^{-1}S_{21}),\tanh(\mu_2^{-1}S_{22})],\quad \mu_2>1.$$

The second Lyapunov function is defined as

$$V_2 = \frac{1}{2}\boldsymbol{S}_2^{\mathrm{T}}\boldsymbol{S}_2. \tag{22}$$

Next, deriving V_2 we get

$$\dot{V}_2 = \boldsymbol{S}_2^{\mathrm{T}}\dot{\boldsymbol{S}}_2. \tag{23}$$

Substituting (20) into (23), we obtain

$$\dot{V}_2 = \boldsymbol{S}_2^{\mathrm{T}}[\boldsymbol{F}_2(\boldsymbol{X}_1,\boldsymbol{X}_2)+\boldsymbol{G}_2(\boldsymbol{X}_2)\boldsymbol{U}+\boldsymbol{D}_2-\dot{\boldsymbol{X}}_{2d}]. \tag{24}$$

Substituting (21) into (24) and using a familiar procedure of the first Lyapunov function in Section 2.1, it is simplified as

$$\dot{V}_2 = \boldsymbol{S}_2^{\mathrm{T}}[-\boldsymbol{k}_2\boldsymbol{S}_2-\boldsymbol{\Lambda}_2\boldsymbol{\Gamma}(\boldsymbol{S}_2)\boldsymbol{S}_2+\boldsymbol{D}_2] \leqslant$$

$$-\lambda_{\min}(\boldsymbol{k}_2)\|\boldsymbol{S}_2\|^2-\lambda_{\min}(\boldsymbol{\Lambda}_2\boldsymbol{\Gamma}(\boldsymbol{S}_2))\|\boldsymbol{S}_2\|^2+$$

$$\|\boldsymbol{S}_2\|\|\boldsymbol{D}_2\| \leqslant -\lambda_{\min}(\boldsymbol{k}_2)\|\boldsymbol{S}_2\|^2-\lambda_{\min}(\boldsymbol{\Lambda}_2)\cdot$$

$$\lambda_{\min}(\boldsymbol{\Gamma}(\boldsymbol{S}_2))\|\boldsymbol{S}_2\|^2+\|\boldsymbol{S}_2\|\rho_2 =$$

$$-[\lambda_{\min}(\boldsymbol{k}_2)+\lambda_{\min}(\boldsymbol{\Lambda}_2)\lambda_{\min}(\boldsymbol{\Gamma}(\boldsymbol{S}_2))]\|\boldsymbol{S}_2\|^2+\|\boldsymbol{S}_2\|\rho_2. \tag{25}$$

In (25), relation between $\|\boldsymbol{S}_2\|$ and $\dot{V}_2$ is described with a mono basic quadratic inequation. Similarly, it is known that $\dot{V}_2 \leqslant \tau_2$ (τ_2 is a bounded and positive number) can be true by designing suitable parameters $\boldsymbol{k}_2$, $\boldsymbol{\Lambda}_2$, μ_2 of that actual controller.

Select the parameters of an actual controller using the similar method as that in Section 3.1. Next, applying them to obtain $\dot{V}_2 \leqslant \tau_2$, we aquire

$$\begin{cases} \lambda_{\min}(\boldsymbol{k}_2) > \lambda_{\min}(\boldsymbol{\Lambda}_2) > 0 \\ \dfrac{\rho_2^2}{4[\lambda_{\min}(\boldsymbol{k}_2)+\lambda_{\min}(\boldsymbol{\Lambda}_2)\lambda_{\min}(\boldsymbol{\Gamma}(\boldsymbol{S}_2))]} = \tau_2 \end{cases}. \tag{26}$$

If $\|\boldsymbol{S}_2\| > \dfrac{\rho_2}{\lambda_{\min}(\boldsymbol{k}_2)+\lambda_{\min}(\boldsymbol{\Lambda}_2)\lambda_{\min}(\boldsymbol{\Gamma}(\boldsymbol{S}_2))}$, there is

$$\dot{V}_2 < 0. \tag{27}$$

If $\|\boldsymbol{S}_2\| \leqslant \dfrac{\rho_2}{\lambda_{\min}(\boldsymbol{k}_2)+\lambda_{\min}(\boldsymbol{\Lambda}_2)\lambda_{\min}(\boldsymbol{\Gamma}(\boldsymbol{S}_2))}$, there is

$$\dot{V}_2 \leqslant \tau_2. \tag{28}$$

Hence, under effects on this actual control law, tracking error $\boldsymbol{S}_2$ can converge to its small neighborhood, and it is

$$\|\boldsymbol{S}_2\| \leqslant \frac{\rho_2}{\lambda_{\min}(\boldsymbol{k}_2)+\lambda_{\min}(\boldsymbol{\Lambda}_2)\lambda_{\min}(\boldsymbol{\Gamma}(\boldsymbol{S}_2))}. \tag{29}$$

3.3 Design of AS

To compensate for errors caused by input constraints, we design this following AS:

$$\dot{\boldsymbol{E}} = \begin{cases} -\boldsymbol{k}_n\boldsymbol{E}-\dfrac{1}{\|\boldsymbol{E}\|^2}[\|\boldsymbol{S}_2^{\mathrm{T}}\boldsymbol{G}_2(\boldsymbol{X}_2)\Delta\boldsymbol{u}\|+ \\ \qquad b_e\Delta\boldsymbol{u}^{\mathrm{T}}\Delta\boldsymbol{u}]\boldsymbol{E}, \quad \|\boldsymbol{E}\| \geqslant \sigma \\ 0, \quad \|\boldsymbol{E}\| < \sigma \end{cases} \tag{30}$$

where

$$\boldsymbol{E} = [E_1 \quad E_2]^{\mathrm{T}},\quad \Delta\boldsymbol{u} = \mathrm{sat}(\boldsymbol{U})-\boldsymbol{U} = [\Delta u_1 \quad \Delta u_2]^{\mathrm{T}},$$

$$\sigma>0, \boldsymbol{k}_n = \mathrm{diag}[k_{n1},k_{n2}], k_{n1}>0, k_{n2}>0, b_e>0,$$

$\lambda_{\min}(\boldsymbol{k}_n)$ is the minimum eigenvalue of diagonal matrix $\boldsymbol{k}_n$. $\boldsymbol{U}_0$ is the limited value of the rudder angle.

The input variable of AS is $\Delta\boldsymbol{u}$ related to $\mathrm{sat}(\boldsymbol{U})$, and $\boldsymbol{E}$ is the state variable and output variable of AS. Its functions can be divided into two cases as follows:

(i) If $\|\boldsymbol{E}\| < \sigma$, there is no control saturation, and the SMC controller works in a linear control zone, meanwhile, AS does not work at all.

(ii) If $\|\boldsymbol{E}\| \geqslant \sigma$, there is control saturation, and the SMC controller turns out to be in a nonlinear control zone. At the same time, input variable $\Delta\boldsymbol{u} = \boldsymbol{U} - \mathrm{sat}(\boldsymbol{U})$ of AS is not zero, and AS starts working, forcing control errors to decay in a short time.

In case (ii) above, the third Lyapunov function is designed as

$$V_3 = \frac{1}{2}\boldsymbol{E}^{\mathrm{T}}\boldsymbol{E}. \tag{31}$$

Next, deriving V_3 we obtain

$$\dot{V}_3 = \boldsymbol{E}^{\mathrm{T}}\dot{\boldsymbol{E}}. \tag{32}$$

Substituting (30) into (32), we get

$$\dot{V}_3 = \boldsymbol{E}^{\mathrm{T}}\Bigg[-\boldsymbol{k}_n\boldsymbol{E} - \frac{1}{\|\boldsymbol{E}\|^2}[\|\boldsymbol{S}_2^{\mathrm{T}}\boldsymbol{G}_2(\boldsymbol{X}_2)\Delta\boldsymbol{u}\| + b_e\Delta\boldsymbol{u}^{\mathrm{T}}\Delta\boldsymbol{u}]\boldsymbol{E}\Bigg] =$$

$$-\boldsymbol{E}^{\mathrm{T}}(\boldsymbol{k}_n\boldsymbol{E}) - \frac{\boldsymbol{E}^{\mathrm{T}}\boldsymbol{E}}{\|\boldsymbol{E}\|^2}[\|\boldsymbol{S}_2^{\mathrm{T}}\boldsymbol{G}_2(\boldsymbol{X}_2)\Delta\boldsymbol{u}\| + b_e\Delta\boldsymbol{u}^2] =$$

$$-\boldsymbol{E}^{\mathrm{T}}(\boldsymbol{k}_n\boldsymbol{E}) - [\|\boldsymbol{S}_2^{\mathrm{T}}\boldsymbol{G}_2(\boldsymbol{X}_2)\Delta\boldsymbol{u}\| + b_e\Delta\boldsymbol{u}^2] \leqslant$$

$$-\lambda_{\min}(\boldsymbol{k}_n)\|\boldsymbol{E}\|^2 - [\|\boldsymbol{S}_2^{\mathrm{T}}\boldsymbol{G}_2(\boldsymbol{X}_2)\Delta\boldsymbol{u}\| + b_e\Delta\boldsymbol{u}^2]. \tag{33}$$

If $\|\boldsymbol{E}\| \geqslant \sigma$, there is

$$\dot{V}_3 \leqslant -\lambda_{\min}(\boldsymbol{k}_n)\|\boldsymbol{E}\|^2 - [\|\boldsymbol{S}_2^{\mathrm{T}}\boldsymbol{G}_2(\boldsymbol{X}_2)\Delta\boldsymbol{u}\| + b_e\Delta\boldsymbol{u}^2]. \tag{34}$$

In (34), the following two inequations are true:

(i) If $b_e > 0$, $-[\|\boldsymbol{S}_2^{\mathrm{T}}\boldsymbol{G}_2(\boldsymbol{X}_2)\Delta\boldsymbol{u}\| + b_e\Delta\boldsymbol{u}^2] \leqslant 0$ is always true.

(ii) If $\lambda_{\min}(\boldsymbol{k}_n) > 0$, $-\lambda_{\min}(\boldsymbol{k}_n)\|\boldsymbol{E}\|^2 \leqslant 0$ is always true.

Hence, under this condition of $\|\boldsymbol{E}\| \geqslant \sigma$, there is $\dot{V}_3 \leqslant 0$, which indicates gradual-approach convergence of AS.

4. Simulation results and analysis

4.1 Simulation conditions

In this section, to demonstrate the performance and feasibility of the proposed SMC and AS, from flight trajectory of a rolling-missile, we select dynamic coefficients on a certain feature point shown in Table 2, where a rolling-missile flies at a speed of 290 m/s and at an altitude of 5 357 m.

Table 2 Dynamic coefficients of a certain feature point

Coefficient	a_{22}/s^{-1}	a_{24}/s^{-2}	a_{25}/s^{-2}	a_{34}/s^{-1}	a_{35}/s^{-1}	a'_{27}/s^{-2}	a'_{28}/s^{-1}
Value	−1.164	−88.22	27.479	0.198 1	0.027 4	−8.823	0.068 1

Our simulation goals in this section are as follows:

(i) In order to verify the anti-interference ability of the proposed SMC law, there are 30% parameter perturbation in this simulation environment.

(ii) To testify the effectiveness of the proposed AS controller, comparative simulation examples are the proposed SMC and the proposed AS combined with SMC.

Hence, the following simulation schemes are needed:

Scheme (i): SMC;

Scheme (ii): SMC+30% parameter perturbation;

Scheme (iii): SMC+AS.

Control parameters are listed as follows:

(i) SMC parameters are as follows:

$$k_{11} = k_{12} = 20, \quad \mu_1 = 2, \quad \Lambda_{11} = \Lambda_{12} = 18,$$

$$k_{21} = k_{22} = 50, \quad \mu_2 = 5, \quad \Lambda_{21} = 20, \quad \Lambda_{22} = 50.$$

(ii) AS parameters are as follows:

$$\boldsymbol{U}_0 = [15/57.3 \quad 15/57.3]^{\mathrm{T}},$$

$$\sigma = 0.1, \quad k_{n1} = k_{n2} = 15, \quad b_e = 20.$$

4.2 Simulation results

To verify the control performance, step-function signals are used here. We set the desired overload to $1g$, and the desired angular rate to zero. The rudder angle is limited within −15° to +15°. Simulation results are shown as follows.

Fig. 3 is the SMC surface S_{11} for longitudinal overload.

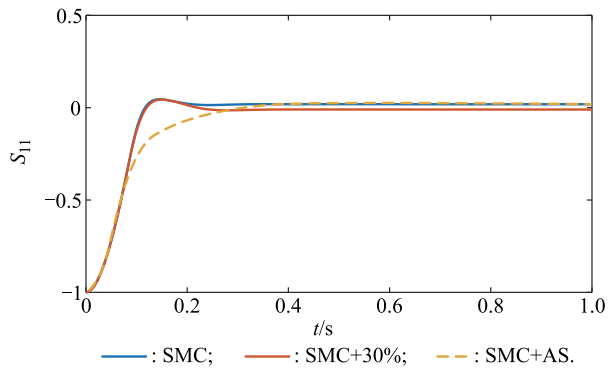

Fig. 3 SMC surface for longitudinal overload

Fig. 4 is the SMC surface S_{12} for lateral overload. Fig. 5 is the SMC surface S_{21} of the pitch angular rate. Fig. 6 is the SMC surface S_{22} for the yaw rate. Fig. 7 shows the rudder angle of the rolling-missile. Fig. 8 shows elevator angle of the rolling-missile. Fig. 9 illustrates the pitch angular rate of the rolling-missile. Fig. 10 illustrates the yaw rate of rolling-missile. Fig. 11 is the step response of longitudinal overload. Fig. 12 is the step response of lateral overload. Fig. 13 shows input variables of AS, and Fig. 14 shows output variables of AS.

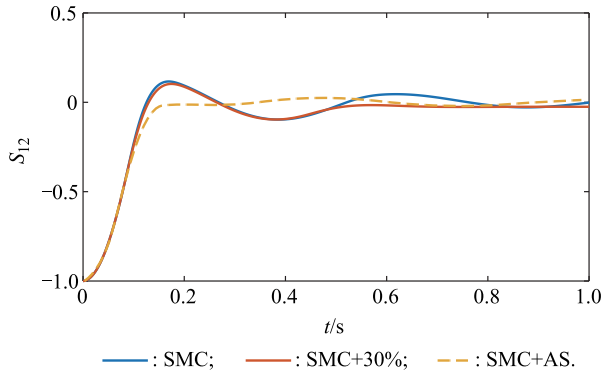

Fig. 4 SMC surface for lateral overload

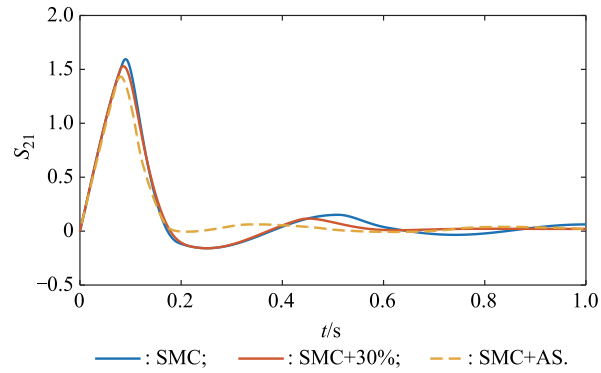

Fig. 5 SMC surface for pitch angular rate

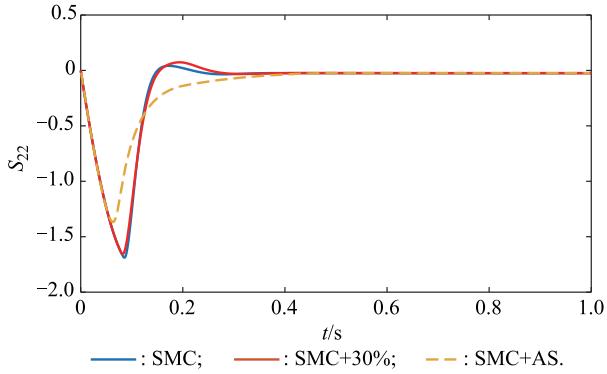

Fig. 6 SMC surface for yaw rate

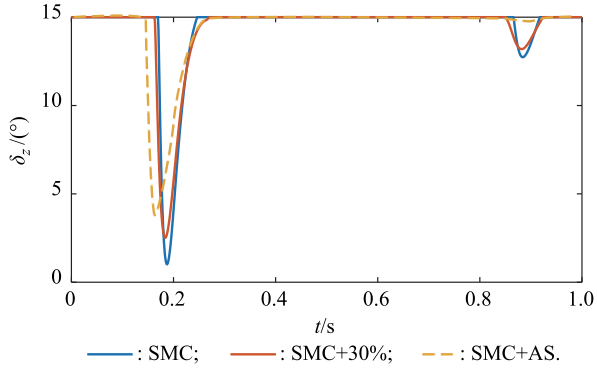

Fig. 7 Rudder angle of rolling-missile

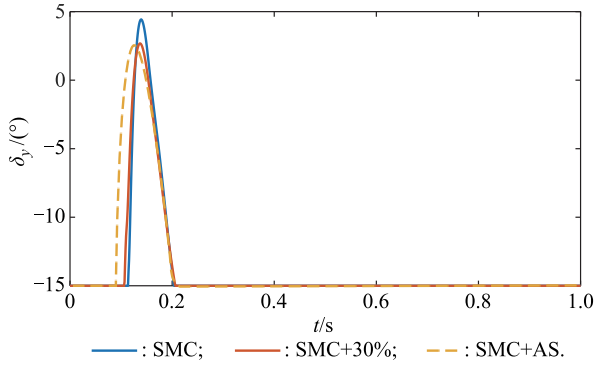

Fig. 8 Elevator angle of rolling-missile

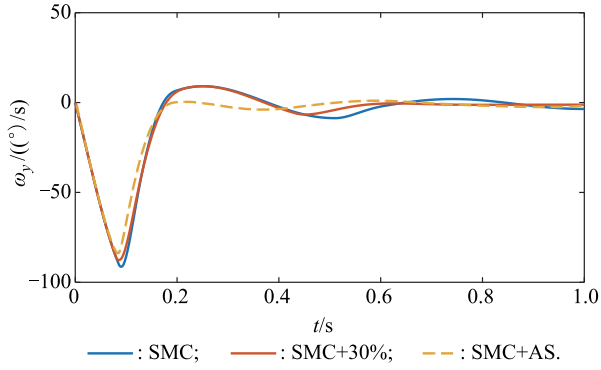

Fig. 9 Pitch angular rate of rolling-missile

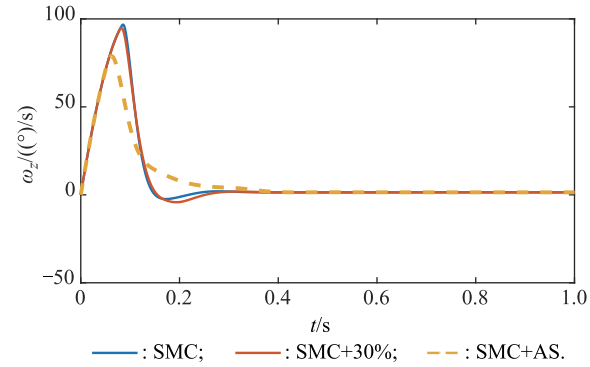

Fig. 10 Yaw rate of rolling-missile

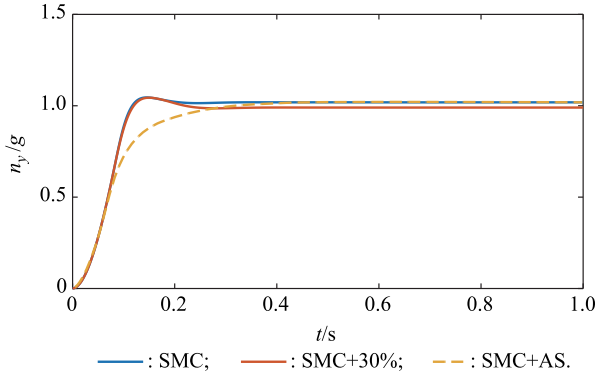

Fig. 11 Longitudinal overload of rolling-missile

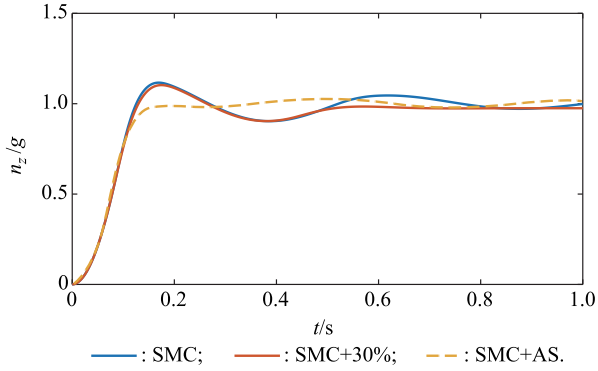

Fig. 12 Lateral overload of rolling-missile

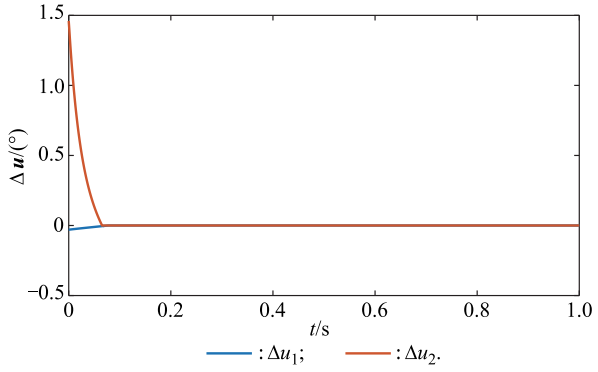

Fig. 13 Input variables of AS (SMC+AS)

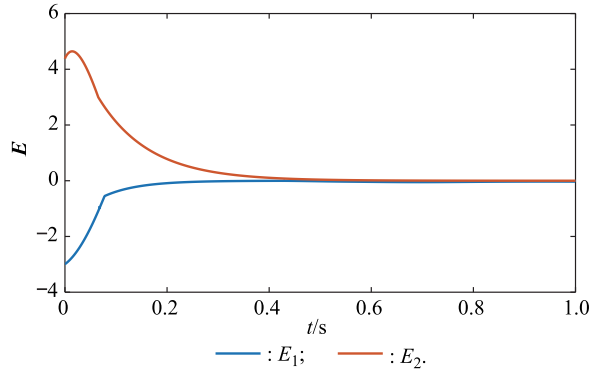

Fig. 14 Output variables of AS (SMC+AS)

4.3 Simulation analysis

4.3.1 Performance of SMC scheme

From simulation results of control scheme (i) and control scheme (ii) showed in Fig. 9 to Fig. 12, we get tracking errors of SMC under 30% parameter perturbation shown in Table 3.

Table 3 Tracking errors of SMC under 30% parameter perturbation %

Longitudinal overload n_y	Lateral overload n_z	Pitch angular rate w_y	Yaw rate w_z
0.02	0.03	1.2	0.5

As is shown in Table 3, tracking errors of this proposed SMC scheme under 30% parameter perturbation are very small, which verifies its strong anti-interference ability.

4.3.2 Performance of AS scheme

From simulation results of these control scheme (i) and scheme (iii), performance of the AS scheme is summarized as follows:

Firstly, definie the sliding-mode surface based on (2), which represents errors of state variables and their desired values. As shown in Fig. 3 to Fig. 6, it can be seen that AS plays an important role in reducing errors of the overload and the angular rate.

Secondly, as shown in Fig. 7, the AS controller makes the rudder angle change slower. Additionally, it reduces amplitudes of the elevator angle shown in Fig. 8.

In addition, as shown in Fig. 9, AS leads to smaller amplitudes of the pitch angular rate, convergence in a shorter time, and decrease of fluctuation. Furthermore, it makes amplitudes of the yaw rate reduce shown in Fig. 10.

Moreover, as shown in Fig. 11 and Fig. 12, we obtain its static and dynamic performance indexes of longitudinal overload and lateral overload respectively in Table 4 Table 5.

Table 4 Static and dynamic performance indexes of longitudinal overload

Control scheme	Rise time t_r/s	Peak time t_p/s	Setting time t_s/s	Overshot σ/%	Static error
SMC	0.11	0.15	0.09	3	0.02
SMC+30%	0.11	0.15	0.09	4	0.02
SMC+AS	0.15	0.35	0.18	1	0.01

Table 5 Static and dynamic performance indexes of lateral overload

Control scheme	Rise time t_r/s	Peak time t_p/s	Setting time t_s/s	Overshot σ/%	Static error
SMC	0.11	0.17	0.10	10	0.02
SMC+30%	0.11	0.17	0.10	4	0.03
SMC+AS	0.12	0.17	0.11	1	0.01

Compared with these proposed control schemes above, it is illustrated that control scheme (iii) has some superiority, and they are small overshot and static error.

4.3.3 Performance summary

Firstly, in terms of rapidity, the proposed control schemes (i), (ii) and (iii) make dynamic system reach convergence in a single second.

Then, summarize their stability. On the one hand, it is proved based on the Lyapunov theory. On the other hand, simulation tests show that tested curves are smooth.

Moreover, in terms of their robustness, simulation test of control scheme (ii) illustrates that the proposed SMC scheme has some priority in anti-interference quality.

Finally, analyzing their anti-saturation performance, we can see that the AS scheme plays an essential role in compensating for saturation from simulation test of control scheme (iii).

5. Conclusions

In this paper, a promising solution for a rolling-missile subject to uncertainties and input constraints is provided. The key idea behind this solution is to incorporate the AS technique into SMC to compensate for the nonlinear terms arising from input constraints.

Moreover, based on the Lyapunov theory, it is proved that the designed controller can guarantee dynamic stability. Furthermore, the SMC law with the tanh-type switching function can reduce intrinsic vibration. Simulation results demonstrate the effectiveness of this proposed control scheme.

References

[1] DONG C Y, LIU C, WANG Q, et al. Near space vehicle control with tracking performance constraints. Journal of Astronautics, 2019, 40(2): 174 – 181. (in Chinese)

[2] DIAN S Y, HU Y, ZHAO T, et al. Adaptive backstepping control for flexible-joint manipulator using interval type-2 fuzzy neural network approximator. Nonlinear Dynamics, 2019, 97(1): 1567 – 1580.

[3] JIANG X Y, SU C L, XU Y P, et al. An adaptive backstepping sliding mode method for flight attitude of quadrotor UAVs. Journal of Central South University, 2018, 25(3): 616 – 631.

[4] HERMAN C, GORDILLO J L. Spatial modeling and robust flight control based on adaptive sliding mode approach for a quadrotor MAV. Journal of Intelligent & Robotic Systems, 2019, 93(1/2): 101 – 111.

[5] KHALID A, ZEB K, HAIDER A. Conventional PID, adaptive PID, and sliding mode controllers design for aircraft pitch control. Proc. of the IEEE International Conference on Engineering and Emerging Technologies, 2019: 1 – 6.

[6] LIU H B, WANG H P, SUN J L. Attitude control for QTR using exponential nonsingular terminal sliding mode control. Journal of Systems Engineering and Electronics, 2019, 30(1): 191 – 200.

[7] JAMALUDIN Z, CHIEW T H, HASHIM A Y B, et al. An enhancement in control laws of super twisting sliding mode servo drive controller using hyperbolic tangent function and arc tangent smoothing function. Proc. of the Symposium on Intelligent Manufacturing & Mechatronics, 2018: 695 – 703.

[8] ZHANG J Q, REN Z H, DENG C, et al. Adaptive fuzzy global sliding mode control for trajectory tracking of quadrotor UAVs. Nonlinear Dynamics, 2019, 97(1): 609 – 627.

[9] ZHENG X Y, ZHANG H, YAN H C, et al. Active full-vehicle suspension control via cloud-aided adaptive backstepping approach. IEEE Trans. on Cybernetics, 2020, 50(7): 3113 – 3124.

[10] JOSE A G, ANTONIO B, SEBASTIAN D. A practical approach to adaptive sliding mode control. International Journal of Control, Automation and Systems, 2019, 17(10): 2452 – 2461.

[11] VENKATESAN N, RATHINASAMY S, FARIS A, et al. Decentralized fault-tolerant resilient control for fractional-order interconnected systems with input saturation. International Journal of Control, Automation and Systems, 2019, 17(11): 2895 – 2905.

[12] FENG Z X, GUO J G, ZHOU J. Novel prescribed performance controller design for a hypersonic vehicle. Journal of Astronautics, 2018, 39(6): 656 – 663. (in Chinese)

[13] SUN D S, CHEN L, ZHANG G C, et al. The anti-windup controller design for multi-propeller aerostat based on nested saturation function. Proc. of the 37th Chinese Control Conference, 2018: 5029 – 5034.

[14] BAIOMY N, KIKUUWE R. An amplitude- and rate-saturated controller for linear plants. Asian Journal of Control, 2019, 21(6): 1 – 15.

[15] LIANG X L. Limited control of guidance and control integration design. Harbin, China: Harbin Institute of Technology, 2015. (in Chinese)

[16] HU Q L, SHAO X D, ZHANG Y M, et al. Nussbaum-type function based attitude control of spacecraft with actuator saturation. International Journal of Robust and Nonlinear Control, 2018, 28(8): 2927 – 2949.

[17] SHI X C, LIM C C, SHI P, et al. Adaptive neural dynamic surface control for nonstrict-feedback systems with output deadzone. IEEE Trans. on Neural Networks and Learning Systems, 2018, 29(11): 5200 – 5213.

[18] HUSSAIN M, REHAN M, AHN C K, et al. Robust antiwindup for one-sided lipschitz systems subject to input saturation and applications. IEEE Trans. on Industrial Electronics, 2018, 65(12): 9706 – 9716.

[19] LIU P B, YAN P, ÖZBAY H. Design and trajectory tracking control of a piezoelectric nano-manipulator with actuator saturations. Mechanical Systems and Signal Processing, 2018, 111: 529 – 544.

[20] WAN N, YAO W R, FANG X, et al. Partially independent control scheme for spacecraft rendezvous in near-circular orbits. Proceedings of the Institution of Mechanical Engineers, Part G: Journal of Aerospace Engineering, 2019, 233(6): 2250 – 2263.

[21] NI J K, LIU L, HE W, et al. Adaptive dynamic surface neural network control for nonstrict-feedback uncertain nonlinear systems with constraints. Nonlinear Dynamics, 2018, 94(1): 165 – 184.

[22] CHEN J, WANG J Y, WANG W H. Model reference adaptive control for a class of aircraft with actuator saturation. Proc. of the Chinese Control Conference, 2018: 993 – 998.

[23] FORMENTIN S, DABBENE F, TEMPO R, et al. Scenario optimization with certificates and applications to anti-windup de-

sign. Proc. of the 53rd IEEE Conference on Decision and Control, 2014: 2810 – 2815.
[24] HE H L, ZHA M, BIAN S F. Anti-windup compensation design for a class of distributed time-delayed cellular neural networks. Journal of Systems Engineering and Electronics, 2019, 30(6): 1212 – 1223.
[25] WANG S S, FU M Y, WANG Y H. Robust adaptive steering control for unmanned surface vehicle with unknown control direction and input saturation. International Journal of Adaptive Control and Signal Processing, 2019, 33(7): 1212 – 1224.
[26] TAO J W, ZHANG T. Robust adaptive attitude maneuvering and vibration reducing control of flexible spacecraft under input saturation. Transactions of Nanjing University of Aeronautics and Astronautics, 2019, 36(1): 98 – 108.
[27] TAO J W, ZHANG T, NIE Y F. Adaptive prescribed performance control for flexible spacecraft with input saturation and actuator misalignment. Tsinghua Science and Technology, 2019, 24(6): 694 – 705.
[28] CHEN M, GE S S, HOW B V E. Robust adaptive neural network control for a class of uncertain MIMO nonlinear systems with input nonlinearities. IEEE Trans. on Neural Networks, 2010, 21(5): 796 – 812.
[29] CHEN M, GE S S, REN B B. Adaptive tracking control of uncertain MIMO nonlinear systems with input constraints. Automatica, 2011, 47(3): 452 – 465.
[30] HUA S Y. Adaptive control of spin guided projectile with input constraints. Nanjing, China: Nanjing University of Science and Technology, 2018. (in Chinese)
[31] SHI M L, WANG L Y, LI Q S, et al. Adaptive inversion control law design and simulation with BTT missile. Electronics Optics and Control, 2012, 19(1): 38 – 41. (in Chinese)

Biographies

HUA Siyu was born in 1992. She received her M.S. degree in ordnance launch theory and technology from Nanjing University of Science and Technology, Nanjing, China, in 2018. From 2018 to 2019, she was an engineer in the 802 Institute of Shanghai Academy of Space Flight Technology. Her research interests include flight aerodynamics, guidance and control.
E-mail: Rain_HSY@163.com

WANG Xugang was born in 1979. He received his Ph.D. degree in navigation, guidance and control from Northwestern Polytechnical University, Xi'an, China, in 2009. He is a research fellow in School of Energy and Power Engineering, Nanjing University of Science and Technology. His research interests include navigation, guidance and control.
E-mail: wxgnets@163.com

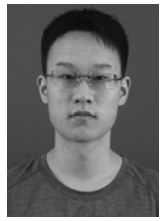

ZHU Yin was born in 1995. He received his M.S. degree in ordnance launch theory and technology from Nanjing University of Science and Technology, Nanjing, China, in 2020. His research interests include flight aerodynamics and control.
E-mail: zynets@163.com